Amyloid fibril length quantification by atomic force microscopy

Wei-Feng Xue

School of Biosciences, University of Kent, Canterbury CT2 7NJ, United Kingdom

Phone +44 (0)1227 824821, fax +44 (0)1227 763912, email w.f.xue@kent.ac.uk

Running title: Amyloid fibril length quantification by AFM

Summary

The biological properties of the highly structured protein aggregates known as amyloid fibrils are intimately related to their length. Detailed information regarding amyloid fibrils' assembly mechanism, functional properties, disease association, and nano-mechanical characteristics can be gained from studies of their length distribution. Such statistical characterization of fibril length will contribute to the future development of improved therapies targeting amyloid associated disease and novel amyloid based nano-materials. Nano-scale microscopy visualization of amyloid fibrils allows the direct measurements of the length of individual fibril particles deposited on surface substrates. However, quantitative characterization of the detailed length distributions of amyloid fibrils in bulk samples is far from straightforward. In this chapter, an atomic force microscopy based method that enables the quantitative characterization of amyloid fibril length distributions in bulk fibril samples is described. Illustrated using amyloid fibril samples generated *in vitro* from β_2-microglobulin, the practical considerations in fibril length distribution determination, including sample preparation, image acquisition, fibril tracing, length dependent bias correction and distribution analysis, are discussed.

Key words:

Amyloid; Length; Length distribution; AFM; Protein misfolding and aggregation; Image analysis; β_2-microglobulin; Single-particle analysis; Size distribution; Fibril fragmentation; Fibril breakage; Protein assembly; Supramolecular assembly; Polymer; Statistical analysis

Background

Amyloid fibrils are highly ordered proteinaceous nano-structures (1-3). Structural examination of *ex situ* amyloid fibrils and fibrils formed *in vitro* reveal that individual fibril particles are typically unbranched structures in the order of ~10 nm wide, and length ranging from few nanometres to many micrometers (e.g. (4-7)). Due to the complex assembly mechanism of amlyloid fibrils that involves nucleation, elongation and fibril fragmentation (8-12), fibril samples are highly heterogeneous with regard to their length (4; 13-20). Environmental factors such as monomer precursor concentration, temperature, pH, and mechanical conditions will affect the length distribution of amyloid fibrils, which in turn will affect fibrils' biological activity through changes in their surface properties and diffusion rate.

Attention has been focused on amyloid due to their association with devastating human diseases such as Alzheimer's, Creutzfeldt-Jakob (CJD), Huntington's and Parkinson's diseases (1). Recently, it has been shown that short amyloid fibril fragments few hundred nm in length or shorter formed from the breakage of long fibrils μm in length have an increased cytotoxic potential compared with their un-fragmented original state (19; 21), indicating that fibril length is an key parameter to be considered for their disease association. Indeed, a number of studies propose fibril length measurements to investigate the connection between amyloid fibrils, their assembly mechanism and their biological and disease associated properties (e.g. (19-23)). Functional amyloid (2) as high-performance nano-materials is a potential emergent engineering application of amyloid fibrils following the recent studies on functional amyloid in nature and amyloid fibrils' favourable nano-mechnical properties (3; 4;

5). Thus, analysis of fibril length can also be employed in characterizing amyloid fibrils designed to exploit their physical properties for engineering purposes.

While measuring the length of individual fibrils deposited on a surface substrate by image analysis is conceptually straightforward, determining the length distribution of amyloid fibril in bulk samples is not. Described in this chapter is a method for determining the bulk sample length distribution of amyloid fibril samples using atomic force microscopy (AFM) imaging, which is a key nano-scale microscopy technique often used for characterising a range of biological polymers (e.g. (24; 25)). The detailed procedures and considerations are illustrated through the length distribution analysis of amyloid fibril samples formed *in vitro* from human β_2-microglobulin (β_2m). These samples of long-straight twisted β_2m fibrils formed under low pH, which display all the hallmarks of amyloid (7; 26; 27), represent an ideal system to demonstrate the steps involved in the determination of fibril length distributions (Fig 1).

Insert Figure 1

Acquiring images for length quantification

Samples containing long-straight amyloid fibrils of human β_2m used for fibril length distribution analysis are grown *in vitro* at pH 2.0 by seeding a freshly prepared 120 μM monomer solution with 0.1% preformed fibril seeds according to established protocols (19). Seeded growth ensures the generation of high quality morphologically homogeneous fibril samples (28) that are well suitable for length distribution analysis. Fibrils samples with different length distributions are generated by mechanical stirring of the seeded samples as described (19). For atomic force microscopy (AFM) imaging in air, fibrils are deposited on

mica (an atomically flat substrate commonly used in AFM) by incubating freshly cleaved mica surface substrate with 20 µL of a solution containing 0.4 µM monomer equivalent concentration of fibrils for 5 min at 25 °C. Great care is taken to minimize additional mechanical perturbations through sample handling and pipetting. The mica surface is subsequently washed with 1 mL sterile-filtered deionised water and dried under a gentle stream of nitrogen gas. Standard tapping mode AFM (TM-AFM) height, amplitude and phase images (Fig 2) are collected using a Dimension 3100 Scanning Probe Microscope (Veeco Instruments) or a MPF-3D Atomic Force Microscope (Asylum Research) using PPP-NCLR cantilever probes (Nanosensors, Neuchatel, Switzerland) with nominal force constant of 48 N/m. All images used for length distribution analysis are collected at 1024x1024 pixels over 10x10 µm surface area and processed using supplied software to remove sample tilt and scanner bow.

Insert Figure 2

In general, height images of surface deposited fibrils for fibril length distribution analysis can be collected on any scanning probe microscopy instrument capable of standard tapping mode operation. The fibril deposition conditions should be optimised so that images contain well-dispersed fibrils of appropriate surface density, allowing for individual fibrils to be found and traced. Large fibril clusters, dense blankets of fibrils or sparse fibril populations should be avoided as much as possible by optimizing the conditions such as protein concentration, ionic strength, incubation time, pH, temperature, and wash procedure. Images for fibril length distribution analysis should ideally be of sufficiently low-magnification wide-area views of the surface with at least 10-20 complete traceable fibrils per image, while still retaining smooth “unpixelated” fibril contours. Because amyloid fibrils tend to be in the order of ~10

nm wide, a resolution of ~0.1-0.2 pixel/nm surface area (corresponding to ~10x10 – 20x20 nm surface areas covered per pixel) will usually yield useful images with fibrils typically appearing 2-5 pixels wide on the images, taken into account tip-sample convolution effects using standard tapping-mode cantilever probes. The surface area scanned per image should also be sufficiently large so that the longest fibrils in a sample can be well contained within the boundaries of the image. Here, for example, 10x10 μm areas are scanned for β_2m fibrils that are up to ~3 μm long. All images collected should be of identical size and resolution for the purpose of subsequent statistical length distribution analysis. To ensure sufficient sampling, a minimum of 3-4 images should be collected per sample.

Single particle measurements of individual fibril length

Once height images of fibrils have been flattened so that tilt and bow effects have been removed, initial single-particle measurements of individual fibril particle lengths can be performed. Contours of fibril particles can be traced and measured directly on height images. Tracing of fibril particles can be performed manually or using software suites that offer semi automatic or automatic tracing functions (examples in (4; 18; 20)). Here, β_2m fibrils are traced using automated scripts written in Matlab (Fig 3). While it is straightforward to trace and measure individual fibrils that are well separated from clusters or at least do not have too many overlaps with other fibrils, not all fibrils can be traced even on well-dispersed images. Examples of such un-traceable fibril particles include fibrils in clusters with too many complex crossovers with other fibrils (e.g. I in Fig 3) and fibrils not fully within the bounds of the image (e.g. II in Fig 3). The omission frequency of such fibril particles is length dependent and will have an impact on the subsequent length distribution analysis, which will be discussed later. Also omitted in the single particle analysis are apparent spherical particles

(e.g. III in Fig 3). These particles likely represent small fibril particles with length that are too short to be determined using the image resolution settings employed. Their length, therefore, denote the lower limit of length that can be determined under a given image resolution. For example, under the imaging conditions employed here for β_2m fibrils, fibril particles shorter than ~20 nm in length cannot be determined reliably.

Insert Figure 3

Because fibril length distribution analysis is a single particle method, a large number of individual fibril particle measurements must be obtained in order to construct useful and meaningful length distributions. The number of fibrils that can be traced and their length measured per image depend on the length of the fibrils in relation to the surface area covered by the images. Because the surface area imaged and image resolution must be kept constant for each image for the purpose of subsequent length distribution analysis, samples containing long fibrils relative to the image dimensions will require larger number of images compared with samples containing fibrils much shorter than the image dimensions. In general, at least few hundred individual fibril lengths should ideally be obtained per sample. This could translate into ~10-20 or more images required for length distribution analysis per sample if 10-20 fibrils are fully traceable per image.

Prior to length distribution analysis, the morphological properties of the fibrils should be checked by analysis of fibril heights, which represent the apparent width of surface deposited fibrils. The height along a traced contour of a β_2m fibril is show in Fig 4. The height profile (Fig 4A) shows periodic behaviour consistent with their twist observed by transmission electron microscopy (Fig 4B, (7)). The height distribution of the height of fibrils contours

obtained from a typical β_2m sample (Fig 4C) shows expected absence of additional peaks that would indicate significant populations of fibrils of different types. More importantly here, fibril height distribution is consistent across different fibril samples independent of fibril length (Fig 5). Together, these controls suggest that samples containing the same type of long-straight twisted β_2m fibrils of the same width are analyzed. Thus, subsequent distribution analysis on samples containing fibrils of indistinguishable morphology will likely represent the length distribution of a consistent population.

Insert Figure 4

Insert Figure 5

Distributions of fibril length

The observed surface length distribution of deposited fibrils can be readily obtained and visualized using the measured single particle fibril lengths. Length distributions can be visualized through histograms, which are frequently used to represent probability density estimates. Length distributions should also be represented and visualized by cumulative distribution plots. On cumulative plots, the probability P of finding individual fibrils of length L shorter than the length l is plotted against the length l, as described by the cumulative distribution function (CDF) of fibril lengths, is visualized:

$$\mathrm{CDF}(l) = P(L \le l) = \frac{N(L \le l)}{N_{tot}} \qquad \text{Eq. (1)}$$

In Eq. (1), $N(L \leq l)$ is the number of fibrils in a sample shorter than the length l, and N_{tot} is the total number of fibril particles measured in the sample. Cumulative distribution plots are complementary to histograms because they do not depend on how the data are binned, unlike histograms. In Fig. 6, the observed surface length distributions of β_2m fibrils from two distinct samples of different length distributions deposited on mica surface are shown as histogram as well as cumulative distribution plot.

Insert Figure 6

Because amyloid fibrils are polymeric structures highly variable in length, the average length of the observed surface deposited fibrils will depend on the method of averaging. The number average length, which is the arithmetic mean length over individual fibrils, can be calculated as:

$$\bar{L}_n = \frac{\sum_i L_i}{N_{tot}} \qquad \text{Eq. (2)}$$

The weight average length, which represents the average fibril length if the mass or the number of monomers per fibril is considered, can be calculated using the following equation:

$$\bar{L}_w = \frac{\sum_i m_i L_i}{\sum_i m_i} = \frac{\sum_i L_i^2}{\sum_i L_i} \qquad \text{Eq. (3)}$$

The right hand side of Eq. (3) assumes that the fibril sample analyzed contains fibrils of the same type and, therefore, the same width (Fig 4).

While the surface length distribution of fibrils deposited on a substrate is straightforward to obtain from the individual length measurements, they do not readily represent the fibril length distribution of the bulk samples. The inability to analyze the length of every fibril on images (Fig 3) combined with differences in the efficiency of which fibrils deposit on the surface substrate (Fig 7) will result in a length quantification "efficiency" that is length-dependent. Thus, the probability of a fibril being fully traceable on an image is not only dependent on its population in the bulk sample, but also dependent its own length. Figs 8 and 9A illustrate the length-dependent bias. As seen in Fig 9A, depending on the observed weight average length of traced fibrils on a image, different total mass of fibrils on that image are traced, measured and included in the length distribution analysis despite the same mass concentration of samples were analyzed using identical protocol under the same conditions. The length-dependent bias will, therefore, result in a difference between the observed surface fibril length distribution and the bulk sample fibril length distribution.

Insert Figure 7

Insert Figure 8

A method to correct for the length-dependent bias and to estimate the bulk sample fibril length distribution using the observed surface fibril length distribution has been described (20). Essentially, this method assumes a length dependent weighting factor $w_{bc}(l)$ that describes the relative difference between the probability of detecting and measuring a surface deposited fibril of length L from a sample ($P_{obs}(L=l)$) and the probability of finding a fibril of identical length in the bulk of the same sample ($P_c(L=l)$):

$$w(l) = \frac{P_c(L = l)}{P_{obs}(L = l)}, \qquad P_c(L = l) = w(l) \cdot P_{obs}(L = l) \qquad \text{(Eq. 4)}$$

The bias-correcting factor $w_{bc}(l)$ that can satisfy Eq. 4 can be determined empirically using image data acquired under identical conditions, resolution and size settings, for fibril samples containing the same type of fibrils, the same mass concentration, but fibrils of different length. In this case, the total length of fibril traced on each image should be the same on average, and any deviation is due to length dependent bias to be corrected. The bias-correcting weighting function $w_{bc}(l)$ can be found through iterative least squares analysis to match the above criterion (Fig 9A right plot). For long-straight β_2m fibrils here, a linear $w_{bc}(l)$ bias-correcting function is able to satisfy the above criterion (Fig 9B).

Insert Figure 9

As seen in Fig 9B for β_2m fibrils, the probability of successfully measuring the length of a ~50 nm long fibril on the acquired images is almost 20 times higher than a ~3 μm long fibril, if the same number of particles of fibrils is present in the sample. The chance of observing the length of a ~1 μm fibril on the acquired images is ~2.5 times higher than a ~3 μm long fibril under the same conditions. Thus, for β_2m fibril samples under the conditions employed, w_{bc} compensates the lower probability of successfully measuring the length of a 3 μm fibril compared with shorter fibril particles by giving a 3 μm fibril larger weight in the corrected length distributions. The number and weight average length of the corrected length distributions can be calculated using Eq. (5) and (6) (derived from Eq. (2) and (3), respectively). Figure 10 shows the resulting bias corrected fibril length distributions of the same fibril samples shown in images in Fig 6 compared with the observed surface length distributions of fibrils deposited on mica. As seen in Fig. 10, the sample length distributions for long-straight β_2m fibrils can shift up by as much as ~200 nm in comparison to observed

surface length distributions. These final bias corrected length distributions can be regarded as population distributions estimates of fibril in the bulk samples.

$$\bar{L}_n = \frac{\sum_i w_i L_i}{\sum_i w_i} \quad \text{(Eq. 5)}$$

$$\bar{L}_w = \frac{\sum_i w_i m_i L_i}{\sum_i w_i m_i} = \frac{\sum_i w_i L_i^2}{\sum_i w_i L_i} \quad \text{(Eq. 6)}$$

Insert Figure 10

Prospects of fibril length distribution analysis

The TM-AFM based method presented in this chapter is a single particle and model-independent method of quantifying fibril length distributions that does not require *a priori* knowledge or assumption regarding distribution model, shape information, and/or hydrodynamic properties. The image analysis approach could also be, in theory, applied to images acquired using other techniques such as transmission electron microscopy (TEM). However, TM-AFM results in images of less complexity that contain quantitative height topology information, which makes it an ideal technique for single particle analysis of amyloid fibril length. With the rapid progress in commercial AFM instruments in terms of scanning speed and resolution, fibril length distribution analysis will likely develop into more rapid and automated process in the future, compared with the current implementations. Increase in the resolution capabilities of AFM instruments may further result in means to resolve amyloid samples that contain increasingly more complex mixtures of populations.

Recent investigations into the mechanisms of amyloid assembly ((11; 12; 29)) have suggested a key role for fibril fragmentation process that can generate small fibril species capable of accelerating the growth of amyloid through seeding as well as elicit cytotoxic properties ((19; 21)). Employing the method described here, the decrease in length distribution of β_2m fibril samples has been linked to enhanced ability to seed the formation of new amyloid, and to disrupt lipid membranes (Fig 11).

Insert Figure 11

Fig. 11 shows an example that illustrates the importance of length distribution analysis, where the fibril length distribution is a key property that influences the biological response to these polymeric assemblies inherently heterogeneous in length. The above example also demonstrates that length distribution information reveals the relative particle concentration of fibril samples, a key parameter that must be characterized in order to quantitatively understand amyloid associated disease mechanisms. In summary, given the importance of amyloid fibril length and brittleness, the method presented here will be a powerful tool in protein aggregation research.

Acknowledgments

This work was supported by grants from the Wellcome Trust (Grant 075675) and Biotechnology and Biological Sciences Research Council (BBSRC Grant BB/J008001/1). I thank Sheena Radford and the members of the Radford group for advice throughout the work, and members of the Xue group and Kent Fungal Group (KFG) for helpful comments on the manuscript.

References

1. Chiti F, Dobson CM. Protein misfolding, functional amyloid, and human disease. *Annu Rev Biochem* 2006 75: 333-66.

2. Fowler DM, Koulov AV, Balch WE, Kelly JW. Functional amyloid--from bacteria to humans. *Trends Biochem Sci* 2007 32: 217-24.

3. Knowles TP, Buehler MJ. Nanomechanics of functional and pathological amyloid materials. *Nat Nanotechnol* 2011 6: 469-79.

4. Adamcik J, Jung JM, Flakowski J, De Los Rios P, Dietler G, Mezzenga R. Understanding amyloid aggregation by statistical analysis of atomic force microscopy images. *Nat Nanotechnol* 2010 5: 423-8.

5. Knowles TP, Fitzpatrick AW, Meehan S, Mott HR, Vendruscolo M, Dobson CM, Welland ME. Role of intermolecular forces in defining material properties of protein nanofibrils. *Science* 2007 318: 1900-3.

6. Meinhardt J, Sachse C, Hortschansky P, Grigorieff N, Fandrich M. Abeta(1-40) fibril polymorphism implies diverse interaction patterns in amyloid fibrils. *J Mol Biol* 2009 386: 869-77.

7. White HE, Hodgkinson JL, Jahn TR, Cohen-Krausz S, Gosal WS, Muller S, Orlova EV, Radford SE, Saibil HR. Globular tetramers of beta(2)-microglobulin assemble into elaborate amyloid fibrils. *J Mol Biol* 2009 389: 48-57.

8. Cohen SI, Vendruscolo M, Welland ME, Dobson CM, Terentjev EM, Knowles TP. Nucleated polymerization with secondary pathways. I. Time evolution of the principal moments. *J Chem Phys* 2011 135: 065105.

9. Ferrone FA. Analysis of protein aggregation kinetics. *Methods Enzymol* 1999 309: 256-74.

10. Kashchiev D, Auer S. Nucleation of amyloid fibrils. *J Chem Phys* 2010 132: 215101.

11. Knowles TP, Waudby CA, Devlin GL, Cohen SI, Aguzzi A, Vendruscolo M, Terentjev EM, Welland ME, Dobson CM. An analytical solution to the kinetics of breakable filament assembly. *Science* 2009 326: 1533-7.

12. Xue WF, Homans SW, Radford SE. Systematic analysis of nucleation-dependent polymerization reveals new insights into the mechanism of amyloid self-assembly. *Proc Natl Acad Sci U S A* 2008 105: 8926-31.

13. Ban T, Hoshino M, Takahashi S, Hamada D, Hasegawa K, Naiki H, Goto Y. Direct observation of abeta amyloid fibril growth and inhibition. *J Mol Biol* 2004 344: 757-67.

14. Mossuto MF, Dhulesia A, Devlin G, Frare E, Kumita JR, de Laureto PP, Dumoulin M, Fontana A, Dobson CM, Salvatella X. The non-core regions of human lysozyme amyloid fibrils influence cytotoxicity. *J Mol Biol* 2010 402: 783-96.

15. Pieri L, Madiona K, Bousset L, Melki R. Fibrillar alpha-synuclein and huntingtin exon 1 assemblies are toxic to the cells. *Biophys J* 2012 102: 2894-905.

16. Sun Y, Makarava N, Lee CI, Laksanalamai P, Robb FT, Baskakov IV. Conformational stability of prp amyloid fibrils controls their smallest possible fragment size. *J Mol Biol* 2008 376: 1155-67.

17. Tanaka M, Collins SR, Toyama BH, Weissman JS. The physical basis of how prion conformations determine strain phenotypes. *Nature* 2006 442: 585-9.

18. van Raaij ME, van Gestel J, Segers-Nolten IM, de Leeuw SW, Subramaniam V. Concentration dependence of alpha-synuclein fibril length assessed by quantitative atomic force microscopy and statistical-mechanical theory. *Biophys J* 2008 95: 4871-8.

19. Xue WF, Hellewell AL, Gosal WS, Homans SW, Hewitt EW, Radford SE. Fibril fragmentation enhances amyloid cytotoxicity. *J Biol Chem* 2009 284: 34272-82.

20. Xue WF, Homans SW, Radford SE. Amyloid fibril length distribution quantified by atomic force microscopy single-particle image analysis. *Protein Eng Des Sel* 2009 22: 489-96.

21. Xue WF, Hellewell AL, Hewitt EW, Radford SE. Fibril fragmentation in amyloid assembly and cytotoxicity: When size matters. *Prion* 2010 4: 20-5.

22. Bernacki JP, Murphy RM. Model discrimination and mechanistic interpretation of kinetic data in protein aggregation studies. *Biophys J* 2009 96: 2871-87.

23. Cohen SI, Vendruscolo M, Dobson CM, Knowles TP. Nucleated polymerization with secondary pathways. Iii. Equilibrium behavior and oligomer populations. *J Chem Phys* 2011 135: 065107.

24. Lyubchenko YL, Shlyakhtenko LS, Ando T. Imaging of nucleic acids with atomic force microscopy. *Methods* 2011 54: 274-83.

25. Uversky VN. Mysterious oligomerization of the amyloidogenic proteins. *FEBS J* 2010 277: 2940-53.

26. Gosal WS, Morten IJ, Hewitt EW, Smith DA, Thomson NH, Radford SE. Competing pathways determine fibril morphology in the self-assembly of beta2-microglobulin into amyloid. *J Mol Biol* 2005 351: 850-64.

27. Smith DP, Jones S, Serpell LC, Sunde M, Radford SE. A systematic investigation into the effect of protein destabilisation on beta 2-microglobulin amyloid formation. *J Mol Biol* 2003 330: 943-54.

28. Petkova AT, Leapman RD, Guo Z, Yau WM, Mattson MP, Tycko R. Self-propagating, molecular-level polymorphism in alzheimer's beta-amyloid fibrils. *Science* 2005 307: 262-5.

29. Collins SR, Douglass A, Vale RD, Weissman JS. Mechanism of prion propagation: Amyloid growth occurs by monomer addition. *PLoS Biol* 2004 2: e321.

Figure legends

Fig. 1: AFM and TEM images of long-straight amyloid fibrils formed *in vitro* from human β_2m. (A) A typical 1024x1024 pixel TM-AFM height image of the β_2m fibrils deposited on freshly cleaved mica surface substrate, with the height color scale shown to the right. (B) A typical negative stain TEM image of the β_2m fibrils. A 2.5x-magnified section, and a 10x-magnified section of a single fibril are also shown. The images each cover a surface area of 10x10 μm, with the scale bars representing the length of 2 μm.

Fig. 2: Typical images of the β_2m fibrils deposited on mica acquired from a TM-AFM experiment. Images from the height (A), amplitude (B) and phase (C) channels simultaneously acquired during a TM-AFM experiment are shown together with the color scale of the height image. Images from the three tapping-mode channels provide different modes of contrast representation of the surface deposited fibrils, and the height images are used in subsequent length analysis. The images are 1024x1024 pixel in size and cover a surface area of 10x10 μm. The scale bars represent the length of 2 μm.

Fig. 3: Example of fibril contours traced on an AFM height image. (A) A 1024x1024 pixel, 10x10 μm TM-AFM height image of β_2m fibrils deposited on mica. The scale bar represents the length of 2 μm. (B) Fibril contours that have been traced on the image shown in A using automated MATLAB scripts. (C) Overlay of traced fibril contours in yellow and the image show in A. The roman numerals in A exemplifies fibrils that could not be successfully traced: I shows a cluster of fibrils, II shows a fibril that is not contained within the bounds of the image, and III shows a particle too small to be resolved on the image.

Fig. 4: Analysis of fibril height. (A) The height profile along a single β_2m fibril contour is shown together with the original TM-AFM image section containing the fibril, approximately parallel-oriented to the height profile. (B) The periodic pattern of the height profile is consistent with the twist of the fibril. A fibril section from a negative stain TEM image, comparable in length to the image in A, is shown for comparison. (C) The height distribution of a β_2m fibril sample obtained from a total of 34620 pixels along fibril contours is show. The histogram plot is aligned to with the height profile in A for comparison.

Fig. 5: Comparison of fibril height in relation to their length. (A) Most frequently observed (mode) height along the fibril contour is plotted against their length. A total of 9298 fibrils from samples of different length distributions are included to illustrate that the widths of the fibrils under the conditions employed are not length-dependent. The black line denotes the average modal height of 5.2 nm. Plot is adapted from (20). (B) The height distribution of the heights shown in A.

Fig. 6: Observed surface fibril length distributions of β_2m fibrils deposited on mica. (A) and (D) Sample TM-AFM images showing two distinct samples of β_2m fibrils deposited on mica. The images are 1024x1024 pixel covering 10x10 μm areas, shown with 2.5x-magnified sections. The scale bars represent the length of 2 μm. (B) and (E) Frequency histograms showing the observed length distributions of the fibril samples shown in (A) and (D), respectively. (C) and (F) Cumulative distribution plots showing the observed length distributions of the fibril samples shown in (A) and (D), respectively. The plots are normalized using Eq. (1) to show probability values from 0 to 1. Figure is adapted from (20).

Fig. 7: Length dependent surface deposition efficiency. (A) The deposition efficiency of β_2m fibrils on mica surface substrate shown as the number of pixel or % of total number of pixels (1024x1024 pixels -> 1.049 Mpixel) on height images that are higher than 2 nm as function of the observed weight average length of fibrils traced on the images. Each data point represents one analyzed 1024x1024 pixel, 10x10 μm image, and 76 images are included in total. This plot indicates that lower mass of long fibril samples are deposited onto the mica (lower deposition efficiency) compared with their shorter counterparts despite the same mass concentration of samples were analyzed under the same conditions using identical protocol. Example 1024x1024 pixel, 10x10 μm images of two samples highlighted in (A) are show in (B) and (C). Each image is shown with 2.5x-magnified sections, and scale bars represent the length of 2 μm.

Fig. 8: Length dependent image analysis efficiency. The number of successfully traced and measured fibril on 1024x1024 pixel, 10x10 μm images is plotted against the weight average length of fibrils traced on the images. Each data point represent one analyzed image, and 76 images are included in total.

Fig. 9: Correcting length dependent bias. (A) The total length of traced fibrils on each image normalized by its average value over all images analyzed is plotted against the observed weight average length of traced fibrils on each image. Left plot shows 76 data points each representing one analyzed 1024x1024 pixel, 10x10 μm image before bias correction, demonstrates significant length-dependent bias in the overall efficiency of fibril length measurements. Right plot shows the same 76 images after length dependent bias correction. (B) The experimentally determined bias correction weighting function $w_{bc}(l)$ obtained for β_2m

fibrils on mica surface substrate, used for bias correction shown in A. Figure is adapted from (20).

Fig. 10: Fibril length distributions corrected for length-dependent bias. The bulk sample fibril length distributions of the two β_2m fibril samples shown as blue traces are obtained by bias correcting their observed surface length distribution shown as red traces. (A) and (C) Normalized frequency (unit-area) histograms showing the bulk sample length distributions of the fibril samples shown in Fig. 6 (A) and (D), respectively. (B) and (D) Cumulative distribution plots showing the bulk sample length distributions of the fibril samples shown in Fig. 6 (A) and (D), respectively. The cumulative plots are normalized using Eq. (1) to show probability values from 0 to 1. Figure is adapted from (20).

Fig. 11: Fibril fragmentation reduces the length distribution of β_2m fibril samples and enhances their ability to seed the formation of fibrils and disrupting liposome membranes. This example illustrates the application of fibril length distribution analysis as a powerful tool to study the biological impact of amyloid. (A) Typical TM-AFM height images of the β_2m fibril samples fragmented to different extents by mechanical stirring to different length of time. The left column shows whole 1024x1024 pixel, 10x10 μm image images. The right column shows zoomed in 2x2 μm image regions of the same images. (B) Normalized frequency (unit area) histograms of the sample length distribution of each fibril sample. The number of measured fibril particles (N_{fibril}) is indicated in each histogram. The red text and lines denote the weight average length of each sample with errors corresponding to one standard error. (C) Top: weight average length of β_2m fibrils agitated for different length of time. Middle: the efficiency of the differentially agitated β_2m fibrils to seed new fibril growth characterized by the initial fibril elongation rates. Bottom: the efficiency of the differentially

agitated β_2m fibrils to disrupt liposome membranes of large lamellar vesicles formed from 80% (w/w) phosphatidylcholine and 20% (w/w) phosphatidylglycerol encapsulated with 50 mM carboxyfluorescein. The error bars represent one standard error. Figure is adapted from (19).

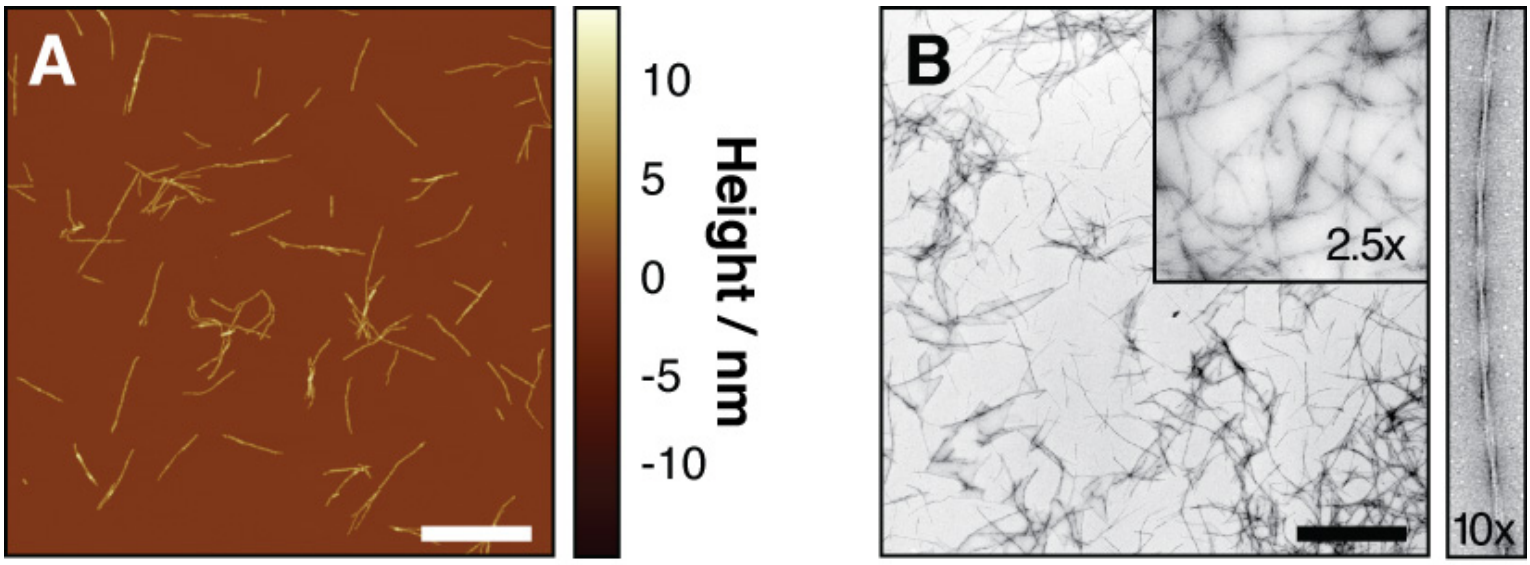
A
10
5
0
-5
-10
Height / nm
B
2.5x
10x

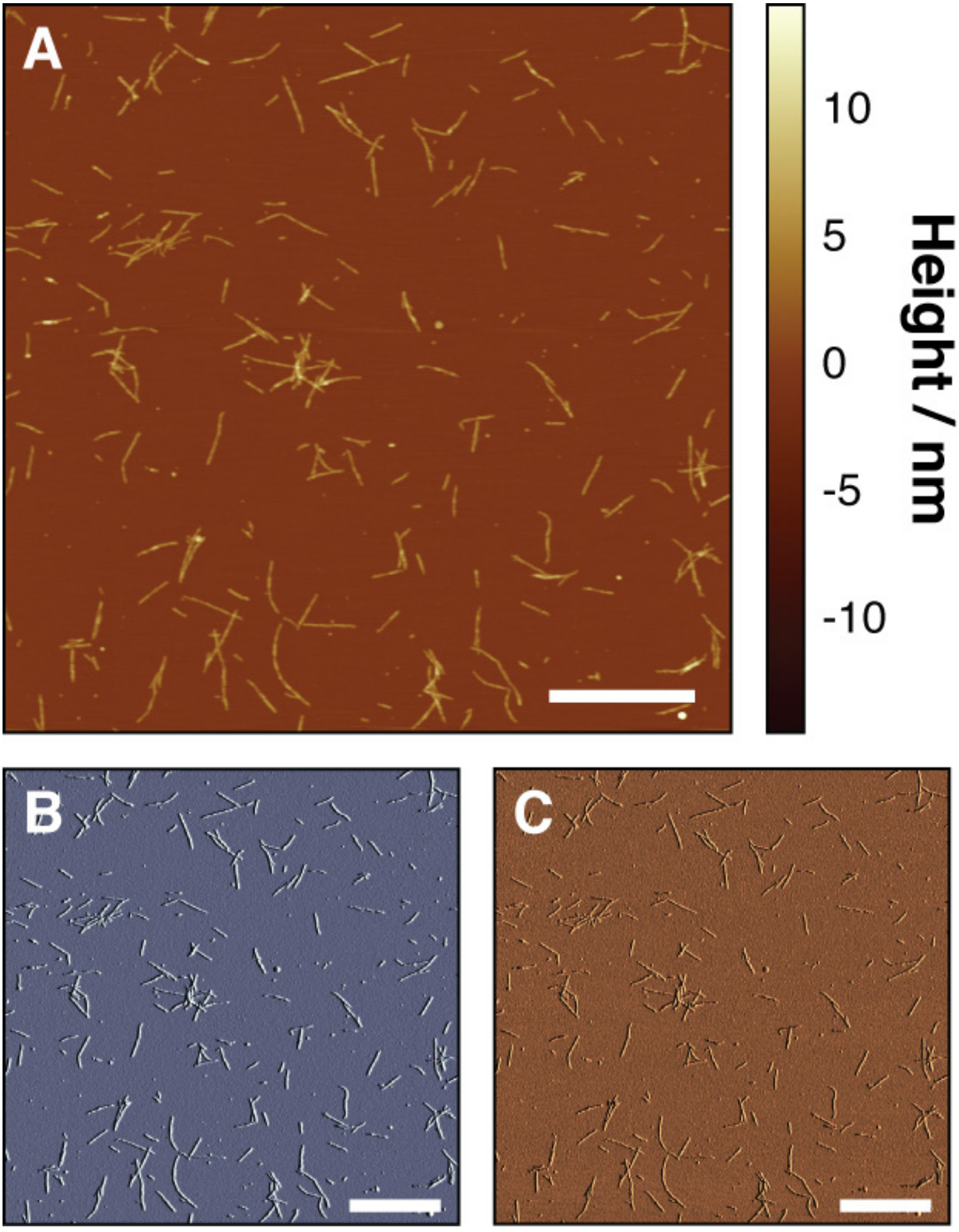
A
B
C
10
5
0
-5
-10
Height / nm

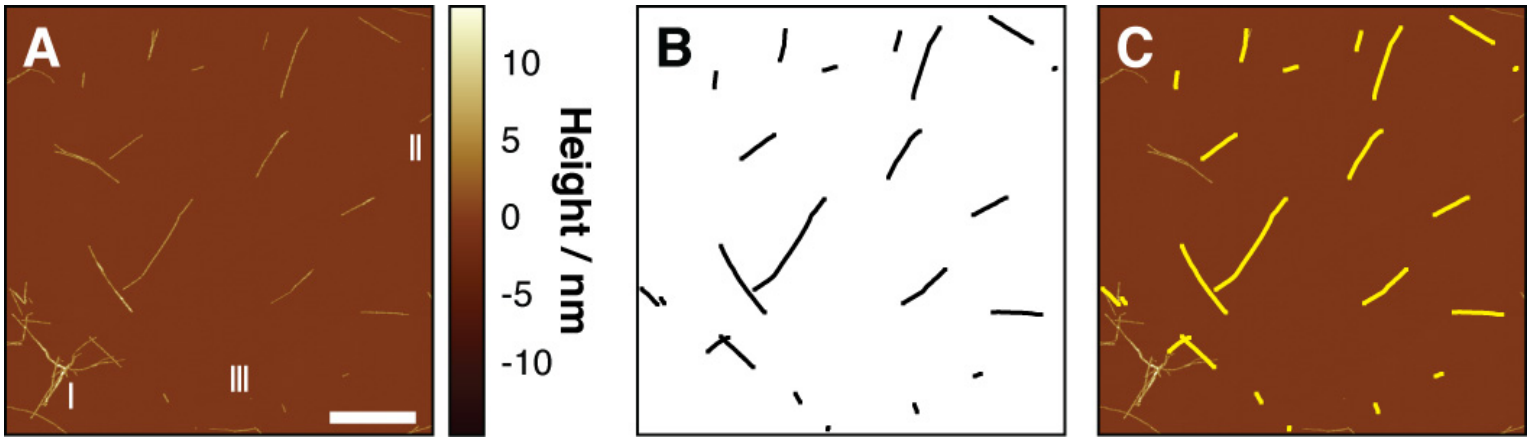
A
I
II
III
10
5
0
-5
-10
Height / nm
B
C

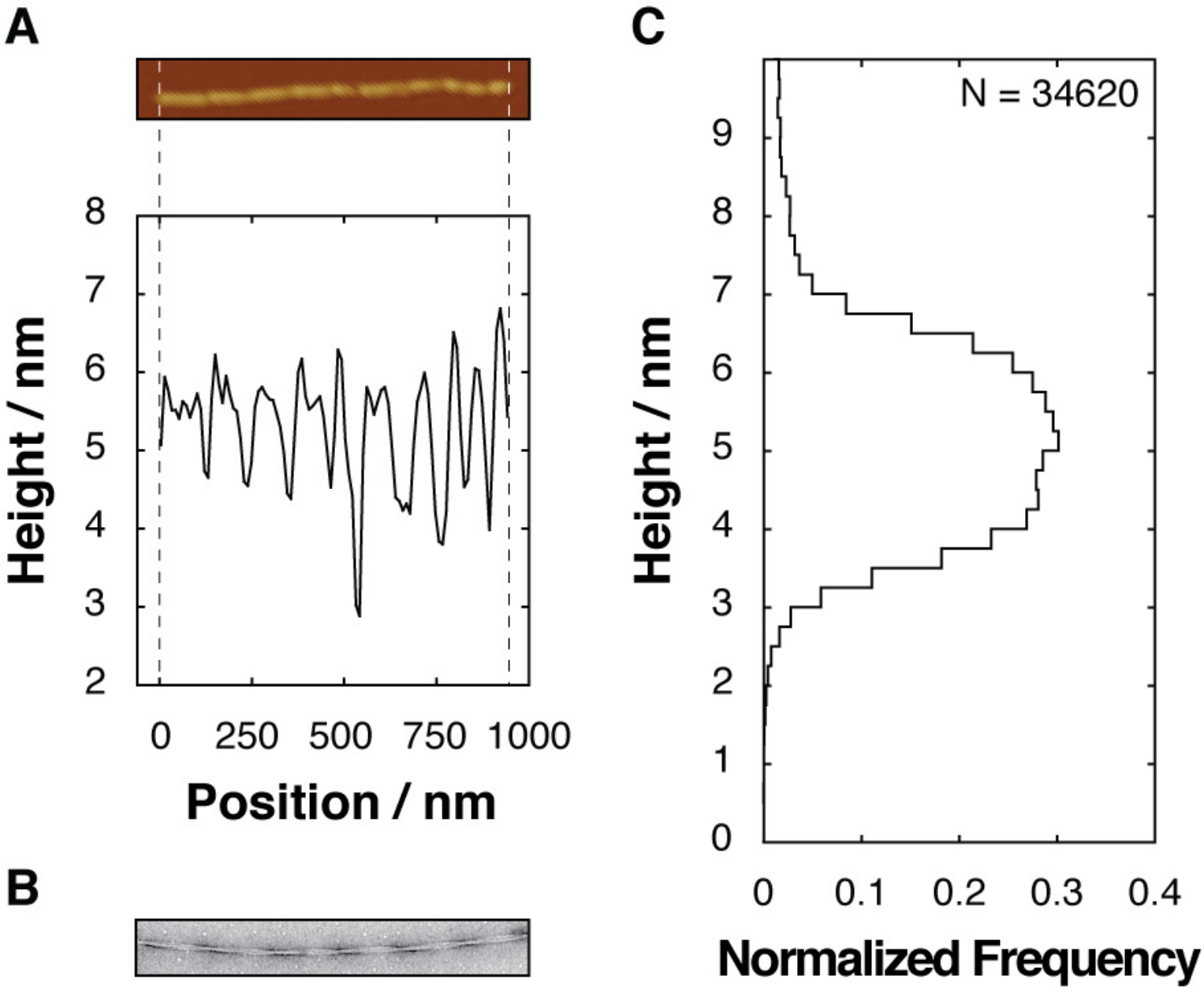
A
B
C
Height / nm
Position / nm
0
250
500
750
1000
2
3
4
5
6
7
8
N = 34620
Normalized Frequency
0
0.1
0.2
0.3
0.4
1
9

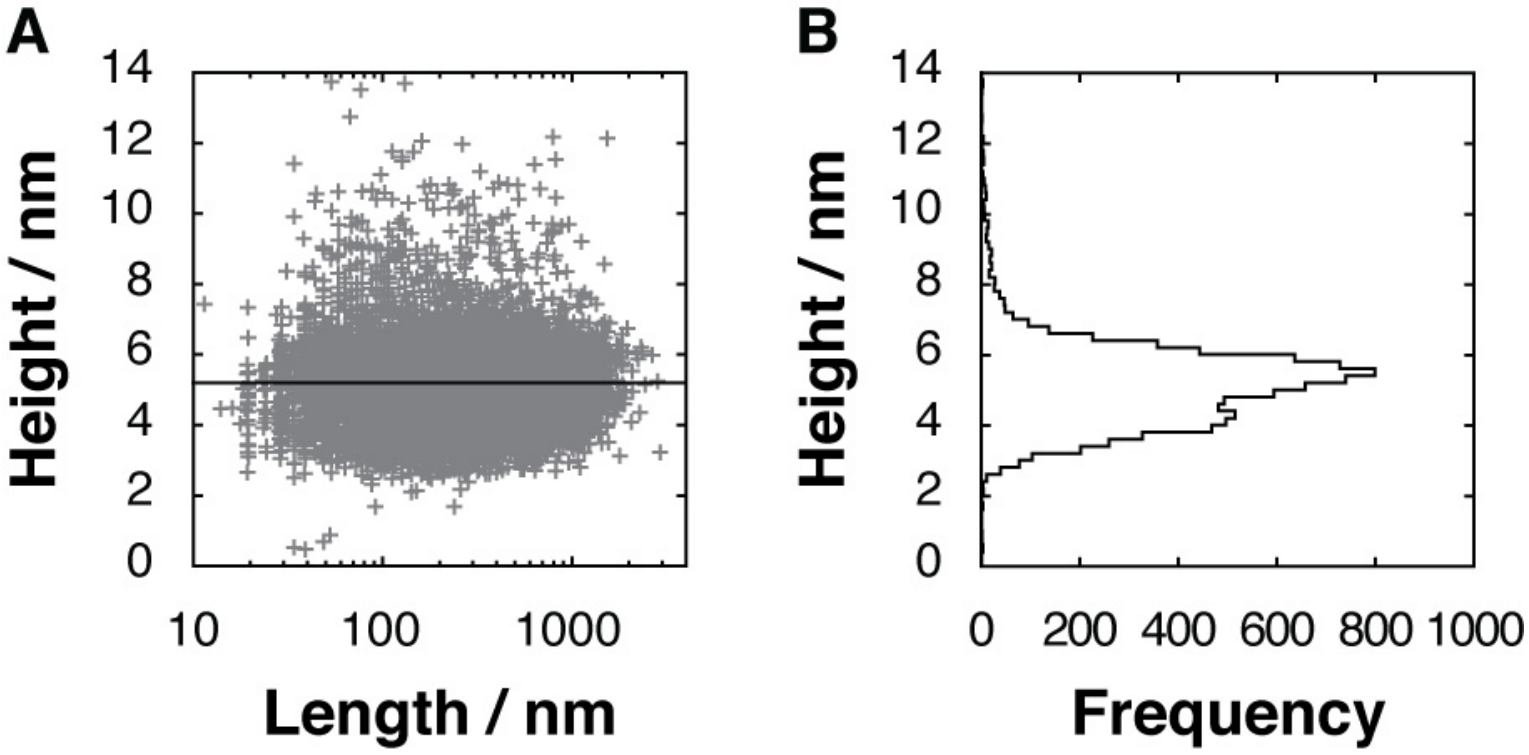
A
Height / nm
14
12
10
8
6
4
2
0
10
100
1000
Length / nm
B
Height / nm
14
12
10
8
6
4
2
0
0
200
400
600
800
1000
Frequency

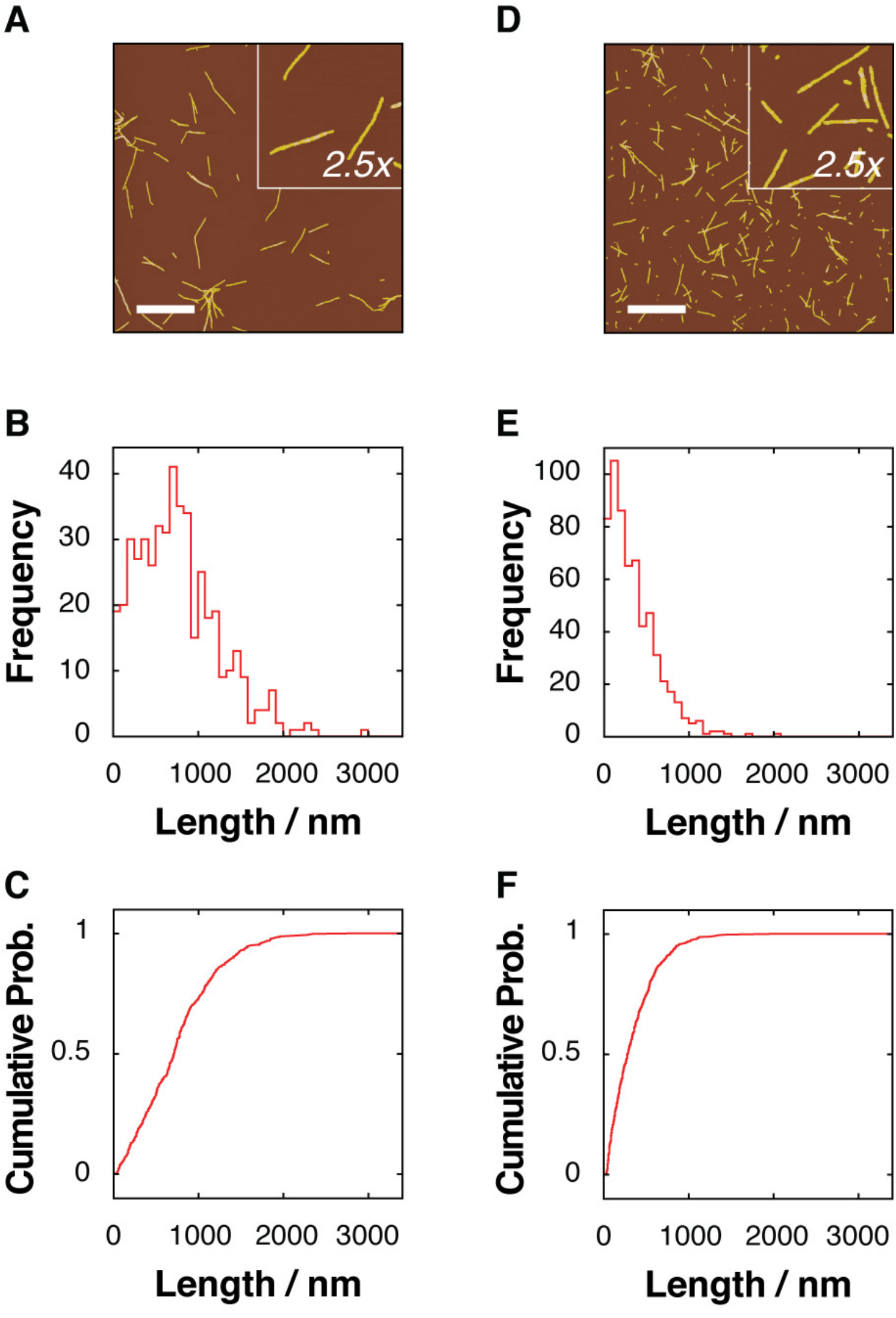
A
2.5x
D
2.5x
B
Frequency
40
30
20
10
0
0
1000
2000
3000
Length / nm
E
Frequency
100
80
60
40
20
0
0
1000
2000
3000
Length / nm
C
Cumulative Prob.
1
0.5
0
0
1000
2000
3000
Length / nm
F
Cumulative Prob.
1
0.5
0
0
1000
2000
3000
Length / nm

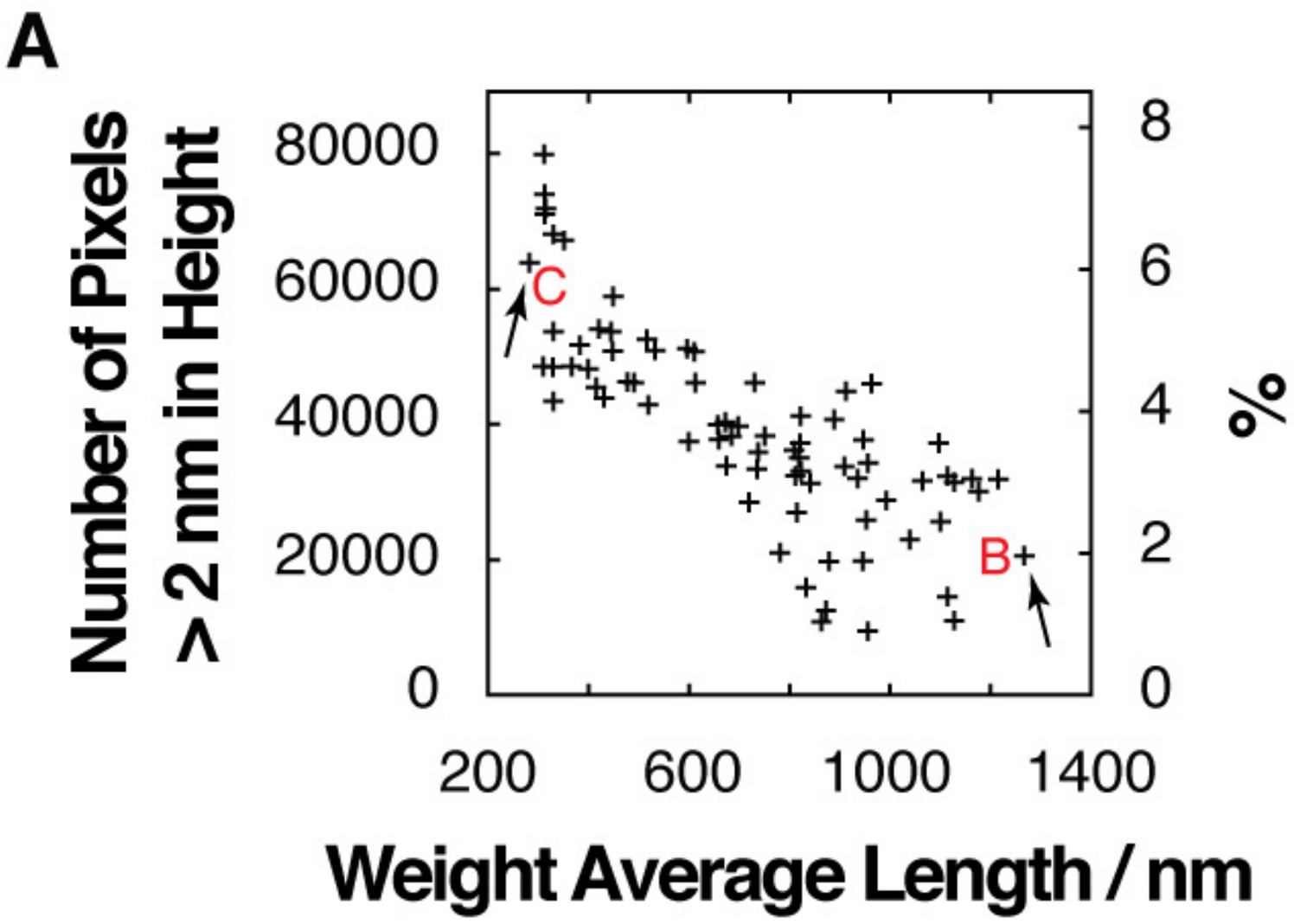
A
Number of Pixels
> 2 nm in Height
80000
60000
40000
20000
0
8
6
4
2
0
%
C
B
200
600
1000
1400
Weight Average Length / nm

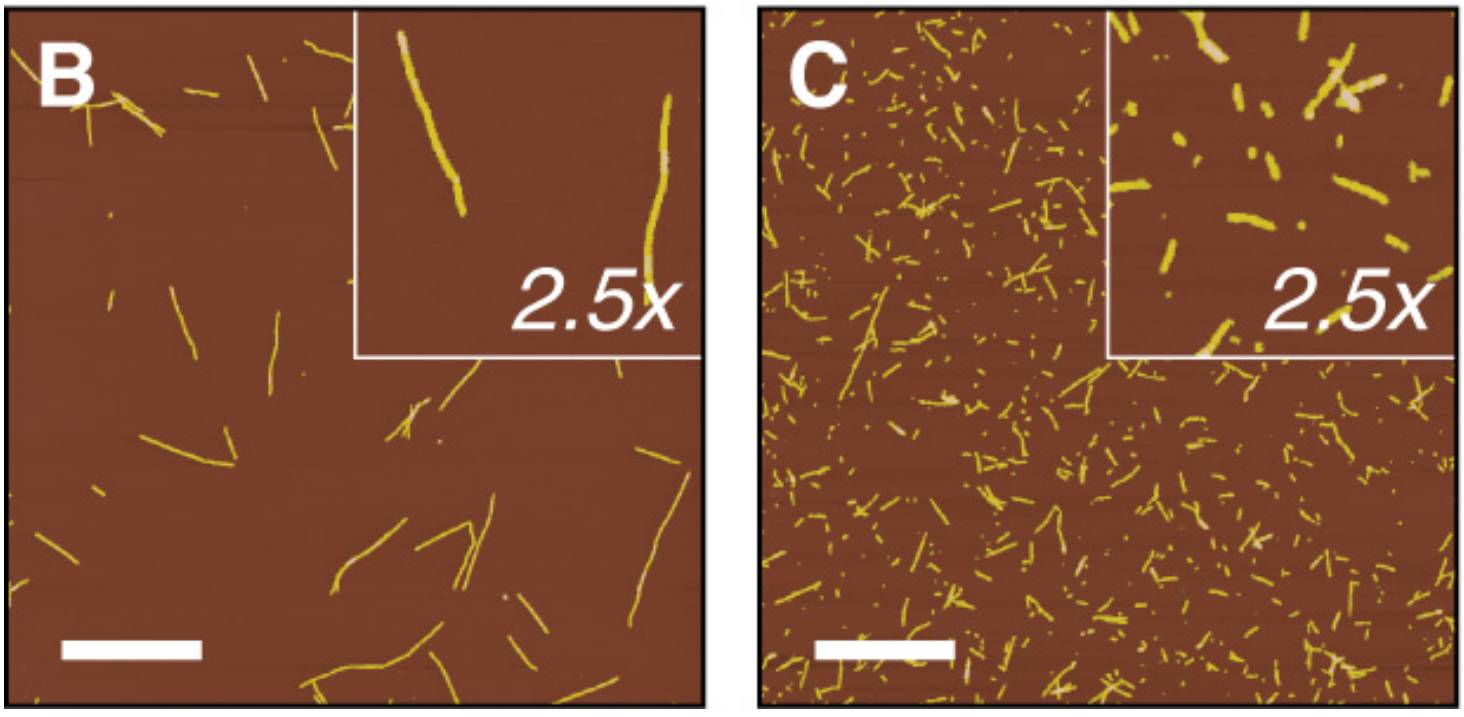
B
2.5x
C
2.5x

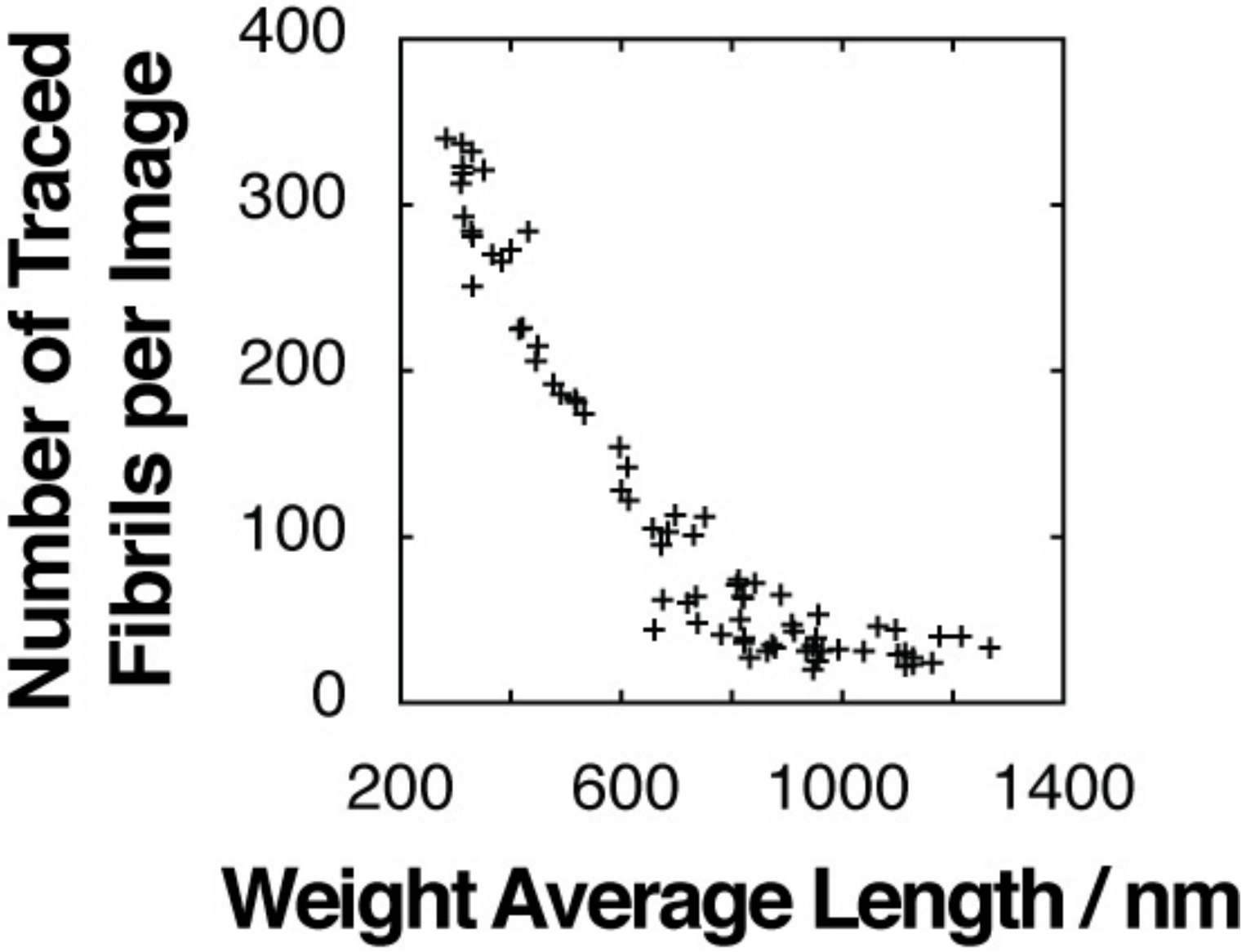
Number of Traced Fibrils per Image
400
300
200
100
0
200
600
1000
1400
Weight Average Length / nm

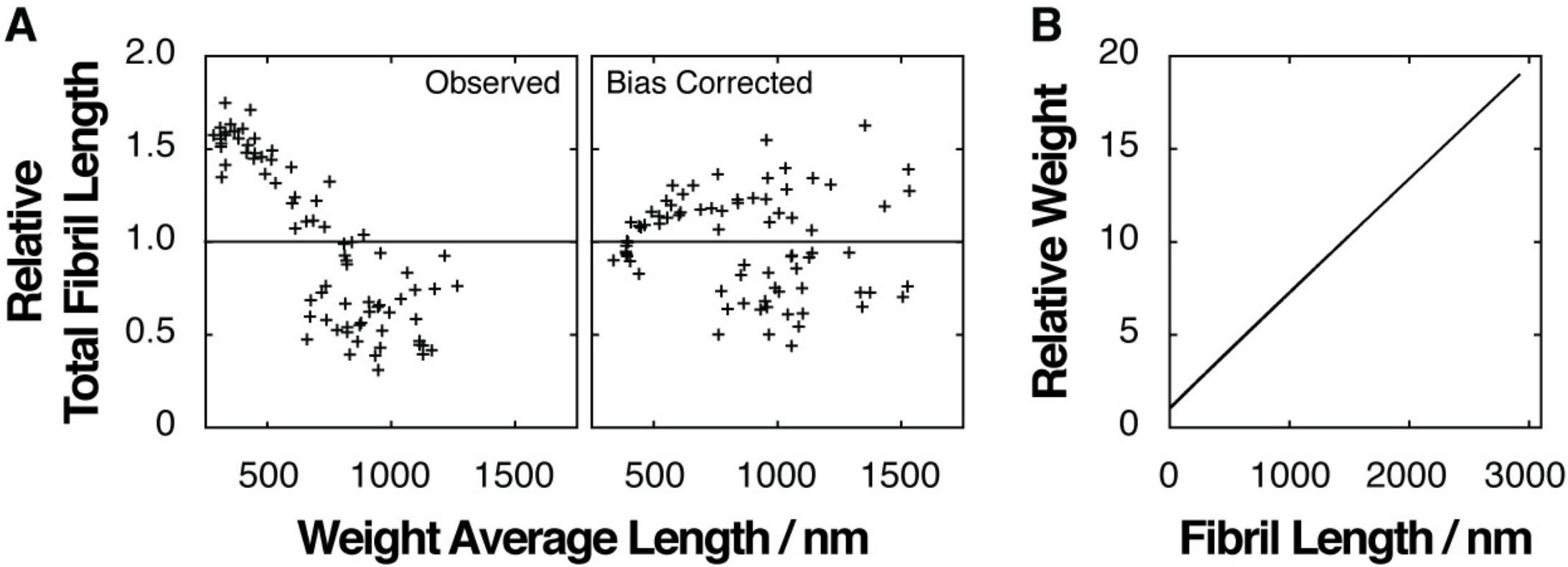
A
Relative Total Fibril Length
2.0
1.5
1.0
0.5
0
Observed
Bias Corrected
500
1000
1500
500
1000
1500
Weight Average Length / nm
B
Relative Weight
20
15
10
5
0
0
1000
2000
3000
Fibril Length / nm

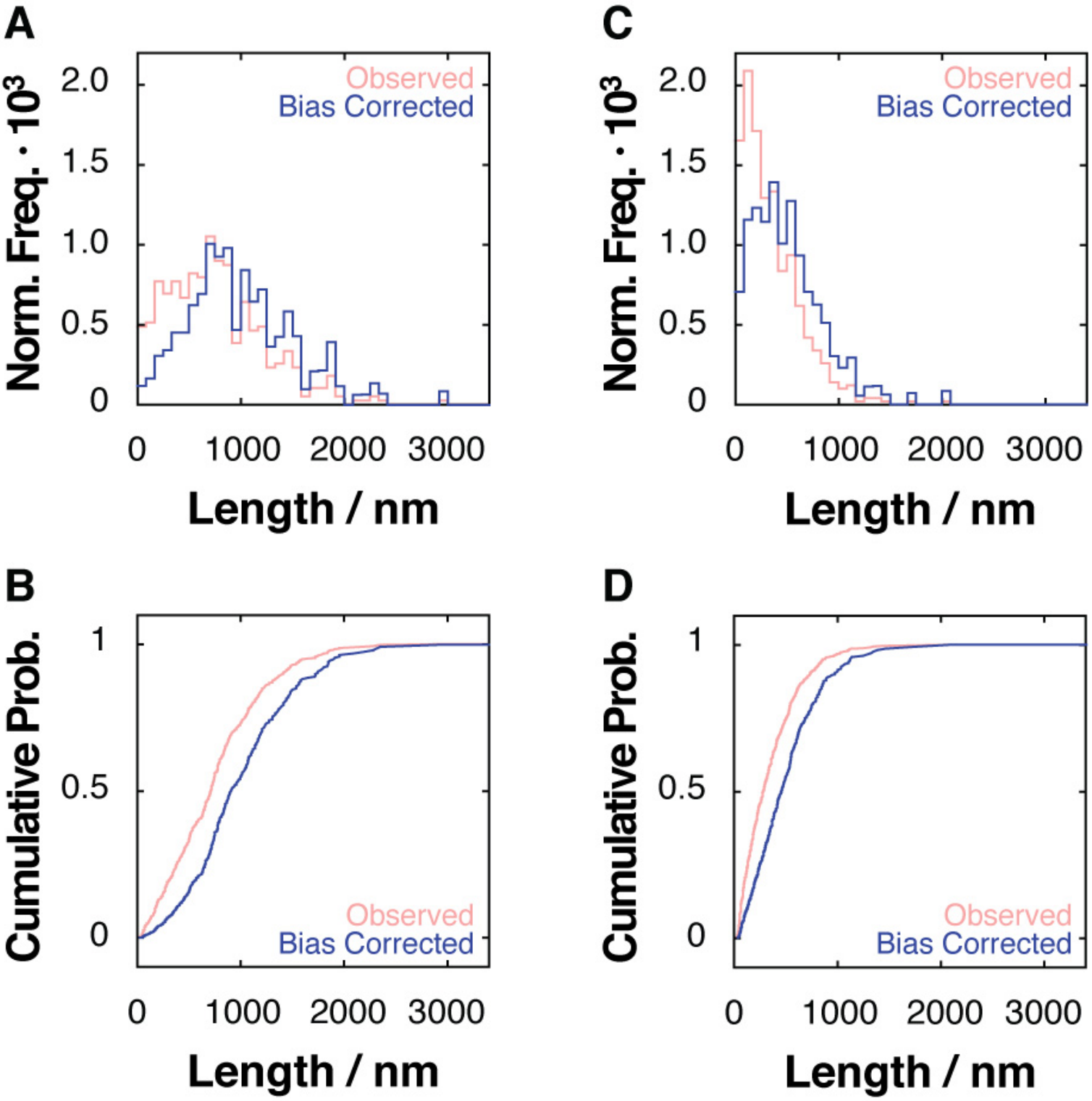
A
Norm. Freq. · 10³
2.0
1.5
1.0
0.5
0
Observed
Bias Corrected
0
1000
2000
3000
Length / nm
C
Norm. Freq. · 10³
2.0
1.5
1.0
0.5
0
Observed
Bias Corrected
0
1000
2000
3000
Length / nm
B
Cumulative Prob.
1
0.5
0
Observed
Bias Corrected
0
1000
2000
3000
Length / nm
D
Cumulative Prob.
1
0.5
0
Observed
Bias Corrected
0
1000
2000
3000
Length / nm

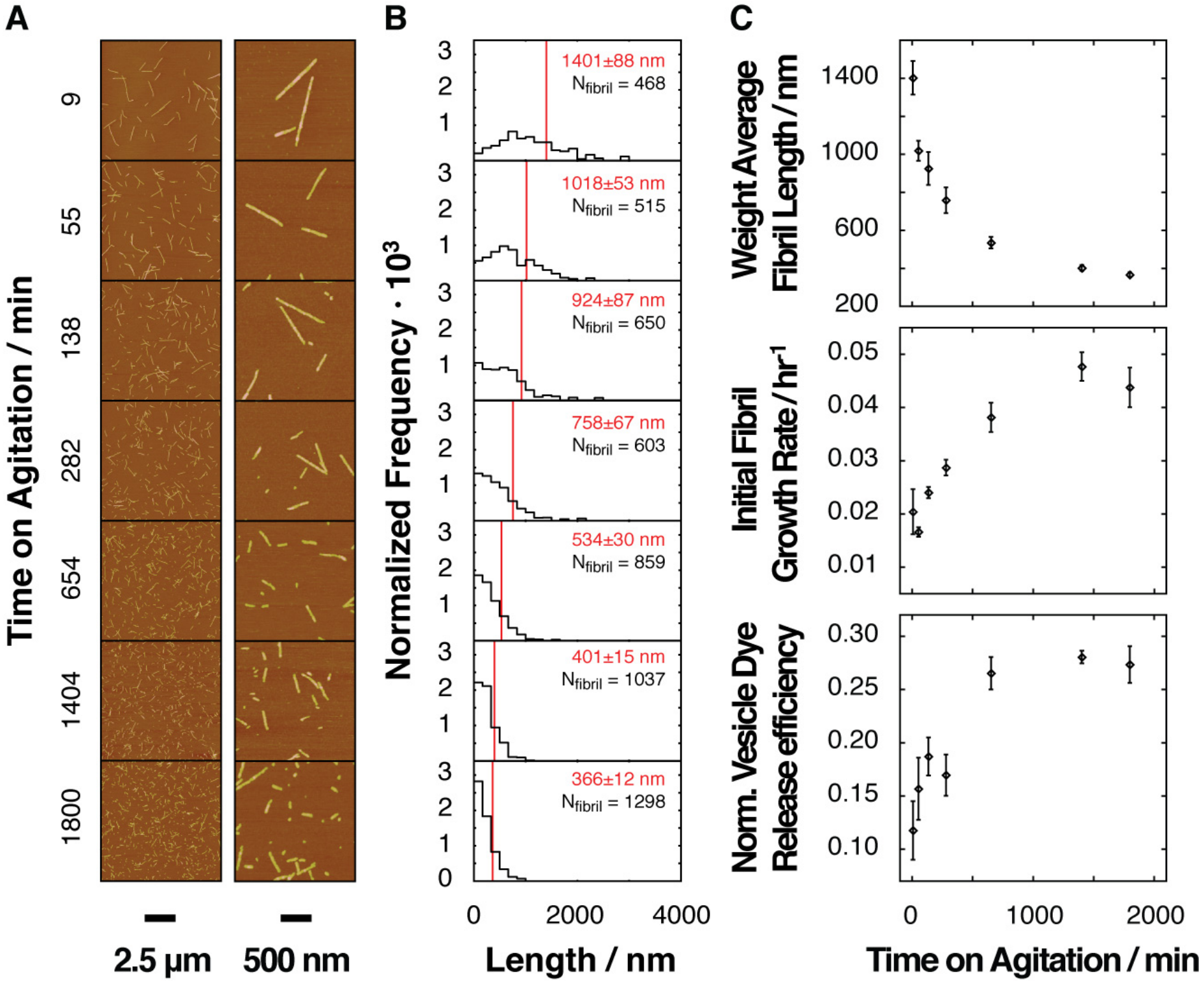
A
Time on Agitation / min
9
55
138
282
654
1404
1800
2.5 µm
500 nm
B
Normalized Frequency · 10³
1401±88 nm
N_fibril = 468
1018±53 nm
N_fibril = 515
924±87 nm
N_fibril = 650
758±67 nm
N_fibril = 603
534±30 nm
N_fibril = 859
401±15 nm
N_fibril = 1037
366±12 nm
N_fibril = 1298
0
1
2
3
0
2000
4000
Length / nm
C
Weight Average Fibril Length / nm
1400
1000
600
200
Initial Fibril Growth Rate / hr⁻¹
0.05
0.04
0.03
0.02
0.01
Norm. Vesicle Dye Release efficiency
0.30
0.25
0.20
0.15
0.10
0
1000
2000
Time on Agitation / min